

Electrophysiological and pro-arrhythmic effects of hydroxychloroquine challenge in guinea-pig hearts

Gongxin Wang¹, Chieh-Ju Lu¹, Andrew W. Trafford², Xiaohui Tian³, Hannali M Flores⁴, Piotr Maj⁵, Kevin Zhang⁶, Yanhong Niu⁷, Luxi Wang¹, Yimei Du⁸, Xinying Ji³, Yanfang Xu⁹, Lin Wu¹⁰, Dan Li¹¹, Neil Herring¹¹, David Paterson¹¹, Christopher L.-H. Huang^{12,14}, Henggui Zhang^{4,12,14}, Ming Lei^{5,14}, Guoliang Hao^{1,11}

Affiliations:

¹Henan SCOPE Research Institute of Electrophysiology Co. Ltd., China

²Unit of Cardiac Physiology, Institute of Cardiovascular Sciences, Manchester Academic Health Sciences Centre, The University of Manchester, UK.

³Department of Pharmacy, Huaihe Hospital and College of Medicine, Henan University, China.

⁴Biological Physics Group, Department of Physics and Astronomy, The University of Manchester, UK

⁵Department of Pharmacology, University of Oxford, Oxford, UK

⁶School of Medicine, Imperial College of London, UK

⁷Fuwai Central China Cardiovascular Hospital, Zhengzhou, China

⁸Department of Cardiology, Union Hospital, Tongji Medical College, Huazhong University of Science and Technology, Wuhan, China

⁹Department of Pharmacology, Hebei Medical University, China

¹⁰Department of Cardiology, Peking University First Hospital, Beijing, China

¹¹Department of Physiology, Anatomy and Genetics, University of Oxford, Oxford, UK

¹²Physiological Laboratory and Department of Biochemistry, University of Cambridge, UK

¹³Peng Cheng Laboratory, Shenzhen, China

¹⁴Key Laboratory of Medical Electrophysiology of the Ministry of Education and Institute of Cardiovascular Research, Southwest Medical University, Luzhou, China

Short title:

Cardiac actions of hydroxychloroquine and azithromycin

Correspondence:

Dr. Gaoliang Hao, Henan SCOPE Research Institute of Electrophysiology Co. Ltd., Kaifeng 475000, China and Department of Physiology, Anatomy and Genetics, University of Oxford, Tel: 008613552324220, Fax: 008613552324220, E-mail: guoliang.hao@epscolab.com

Or Prof. Ming Lei, Department of Pharmacology, University of Oxford, Mansfield Road,
Oxford OX1 3QT, United Kingdom. Tel: 00441865271850; Fax: 00441865271850 E-mail:
ming.lei@pharm.ox.ac.uk

CLHH, HZ, ML and GLH are joint senior authors

Length of Main text: 4999 words

Key points summary.

- *Experimental studies examining electrophysiological actions of hydroxychloroquine (HCQ) were prompted by reported clinical concerns regarding potential cardiac pro-arrhythmic effects particularly when HCQ was combined with azithromycin (AZM) in Covid-19 therapy.*
- *HCQ and (HCQ+AZM) studied over the therapeutic concentration range inhibited hERG and Kir2.1 K⁺ channels expressed in cultured cells, paralleling molecular docking hERG studies*
- *In intact hearts, mapping studies demonstrated that HCQ slowed and disrupted action potential conduction of cardiac excitation, prolonging its duration and the resulting cellular Ca²⁺ signalling, to extents accentuated by AZM inclusion. But these changes caused arrhythmic effects only with the combined (HCQ + AZM) challenge*
- *These novel findings yield possible mechanistic physiological schemes for potentially pro-arrhythmic electrophysiological action of cardiac drugs that extend excitation duration, causing long QT syndrome.*
- *They prompt a requirement for further assessment of HCQ's cardiac safety when variously used for long- or short-term management of both chronic and acute clinical situations.*

ABSTRACT

Hydroxychloroquine (HCQ), clinically established for treating malarial and autoimmune disease, recently initiated cardiac arrhythmogenic concerns in Covid-19 therapy when used alone or with azithromycin (HCQ+AZM). The present experimental investigations of their baseline electrophysiological effects complement existing observational clinical reports. HCQ inhibited I_{Kr} and I_{K1} at therapeutic (10 ± 0.6 and 34 ± 5.0 μM), and I_{Na} and I_{CaL} at higher IC_{50} s, sparing I_{to} and I_{Ks} in patch-clamped HEK293 cells expressing human ion channels. AZM produced minor I_{Na} , I_{CaL} , I_{Ks} , and I_{Kr} inhibition, sparing I_{K1} and I_{to} . (HCQ+AZM) inhibited I_{Kr} and I_{K1} (IC_{50} s: 7.7 ± 0.8 and 30.4 ± 3.0 μM), sparing I_{Na} , I_{CaL} and I_{to} . Molecular induced-fit docking modelling correspondingly confirmed potential HCQ-hERG, but weak AZM-hERG binding. Isolated perfused guinea-pig hearts showed reversibly reduced left atrial and ventricular action potential (AP) conduction velocities and increased conduction heterogeneities on multi-electrode array isochronal, and increased AP durations (APDs) on optical RH237 voltage, mapping, with μM -HCQ challenge. These accompanied bradycardic effects, increased PR and QRS durations, and increased durations and their dispersions, of intracellular $[\text{Ca}^{2+}]$ transients on Rhod-2 mapping. (HCQ+AZM) in combination produced accentuated effects. However, it was (HCQ+AZM) but not HCQ alone that disrupted AP propagation, inducing alternans and torsadogenic-like episodes on voltage mapping during forced pacing protocols. O'Hara-Rudy modelling showed that the observed pharmacological I_{Kr} and I_{K1} effects explained the APD alterations. The latter could explain the prolonged Ca^{2+} transients. These could thence downregulate I_{Na} and AP conduction velocity through recently reported actions of cytosolic $[\text{Ca}^{2+}]$ in a possible scheme describing these HCQ actions, whose clinical implications are discussed.

Key words: Ion channels, Hydroxychloroquine; Azithromycin, cardiac electrophysiology CiPA, COVID-19

INTRODUCTION

The 4-aminoquinolines chloroquine (CQ) and hydroxychloroquine (HCQ) have established, prolonged and extensive, uses as antimalarial prophylactic or therapeutic agents or in management of autoimmune conditions including rheumatoid arthritis and systemic lupus erythematosus (SLE). Their use was recently explored, both by themselves and combined with the antibiotic azithromycin (AZM) in Covid-19 therapy [1, 2]. However, such quinoline

antimalarials and structurally related compounds have long been associated with cardiovascular side effects. In common with Class Ib cardiotropic agents, they modify cardiomyocyte action potential (AP) depolarisation and repolarisation, markedly prolonging action potential durations (APDs), effects clinically indirectly reflected in prolonged electrocardiographic QT intervals [3-5]. They also produce AP conduction effects [6] and are potentially lethal in overdose [7]. Thus, the marked QT prolongations associated with halofantrine therapy have been clearly associated with sudden cardiac death [8, 9]. In addition, CQ and HCQ treatment for rheumatic conditions was associated with conduction disorders in 85% of long-term patients [10].

Nevertheless, the limited available clinical evidence revealed that such electrophysiological changes indeed took place but were not accompanied by major cardiac arrhythmias when employed at the therapeutic CQ and HCQ concentrations associated with rheumatoid arthritis, SLE, and malarial prophylactic therapy [11, 12], suggesting their safety at least with their long established short-term though not necessarily long term use in such conditions (Lane et al., 2020a,b; Hinton, 2020). However, recent use of CQ or HCQ albeit often at increased dosing and further combined with AZM [13] that prompted initial FDA authorization of their emergency use in Covid-19 therapy [14, 15], was followed [1, 2] by concerns about long QT-associated increased cardiac arrhythmic mortality particularly with high dose HCQ combined with AZM [16, 17], but possibly even HCQ alone [18]. These findings prompted FDA cautions against HCQ or CQ use in COVID-19 therapy outside hospital or clinical trial settings [14], and a desirability of accompanying QT interval monitoring [19], whilst not affecting long-established FDA-approved short term uses in malaria, systemic lupus erythematosus (SLE), and rheumatoid arthritis.

However, the latter distinctions could bear on the particular CQ or HCQ dose regimes employed [16], whether they include AZM or otherwise [4, 5, 20], the specific diseases concerned and whether they are associated with systemic cardiac involvement [12, 21, 22], the presence or absence of chronic cardiac conditions and pharmacological effects on the fundamental relationships between observed electrophysiological changes and the presence or absence of pro-arrhythmic effects. For example, delayed ventricular repolarisation, indirectly reflected in prolonged clinical QT intervals, constitutes a sensitive, but is a nonspecific, risk

marker for ventricular tachy-arrhythmic, particularly Torsade de Pointes episodes in turn potentially leading to fatal ventricular fibrillation. However, the physiological relationships between these are incompletely understood [23-25].

We here investigate the electrophysiological effects of HCQ action, administered alone, or combined (HCQ+AZM) with AZM, and the extent to which these lead to pro-arrhythmic changes in expression systems for specific ion channels and baseline healthy hearts. Only limited available controlled experimental studies investigating mechanistic effects, as opposed to observational clinical, studies, of this kind, are available. We first investigated biophysical changes using FDA-recommended Comprehensive in Vitro Proarrhythmia Assay (CiPA) protocols at the single human channel level in HEK293 expression platforms [26]. We next explored drug-channel actions at the molecular level, then demonstrated drug effects on mapping action potential propagation and durations, and Ca^{2+} signalling, during electrocardiographic monitoring in intact perfused guinea-pig hearts. These electrophysiological properties were then correlated with mapping for a presence or otherwise of pro-arrhythmic effects. All experiments compared findings from HCQ and (HCQ+AZM) challenge. O'Hara-Rudy (Ord) modelling studies then could relate biophysical to electrophysiological alterations in action potential recovery properties. The latter could potentially explain observed prolongations of the Ca^{2+} transients. This prompted schemes in which these downregulated I_{Na} and consequently the AP conduction velocities, through recently reported Na^+ channel actions of altered cytosolic $[\text{Ca}^{2+}]$ [27-31]. The relationship of such fundamental physiological findings from normal experimental hearts to clinical situations with or without systemic cardiac involvement could then be discussed.

RESULTS

Patch-clamp studies of single channel characteristics

The first series of experiments assessed the effects of HCQ (Fig. 1) and AZM alone (Fig. 2) and in combination (HCQ+AZM) (Fig. 3) on a range of human cardiac ion channels. The experiments on HCQ and AZM adopted concentrations fully encompassing plasma levels associated with their clinical use. Maintenance stage regimes for the low-dose regime [16] and the initial FDA emergency use authorization (EUA) (<https://www.fda.gov/media/136537/download>) resembled those widely used in antimalarial and autoimmune, systemic lupus erythematosus, therapy for which recent studies reported 1.15-4.5 [32] and 0.5-0.7 μM blood levels [33]. These contrast with the three times greater high-dosage (H)CQ regime allowing for a 2-3 times higher blood concentration, and information at toxic overdose levels exemplified by one at 8.8 mg/L (20.24 μM) [34]. Our explored HCQ range (0.01-100 μM) thus fully encompassed these clinical concentrations, which also provided lower and upper limit HCQ concentrations explored in the subsequent physiological experiments. The biophysical experiments examined inward, cardiac channel currents from hNav1.5 (I_{Na} , A), Cav1.2 ($I_{\text{Ca,L}}$, B), mediating or maintaining membrane action potential depolarization. They also studied outward Kv4.3 (I_{to} , C), hERG (I_{Kr} , C), KCNQ1/E1 (I_{Ks} , E) and Kir2.1 (I_{K1} , F) normally mediating action potential recovery. This encompassed the range of ion channels recommended by the FDA Comprehensive In Vitro Proarrhythmia Assay (CiPA) protocol.

Figure 1 (left panels, i) exemplifies observed ionic currents in the presence of 0, 1, 10 and 100 μM HCQ, using related voltage clamping protocols summarized in the Figure insets. Five concentrations ranging from 10^{-8} to 10^{-4} M were tested for each current examined in 3 to 6 cells at each concentration. Mean concentration-response plots (right panels, ii) used the maximum magnitudes of each current. Where applicable, the consequent alterations in such current magnitudes following pharmacological challenge were used to derive IC_{50} values. Figure 1 (right panels, ii) plots mean ($\pm\text{SEM}$) fractional reductions in current magnitude against HCQ concentration for I_{Na} (A), $I_{\text{Ca,L}}$ (B), I_{to} (C), I_{Ks} (D), I_{Kr} (E) and I_{K1} (F). μM -HCQ inhibited both I_{Kr} -tail and I_{K1} pulse currents with IC_{50}s of 10 ± 0.6 μM (D) and 34 ± 5 μM (F), respectively, with more marked effects on I_{Kr} . μM -HCQ had less effect on I_{Na} and $I_{\text{Ca,L}}$ with IC_{50}s of 113 ± 78

μM and $209 \pm 94 \mu\text{M}$ respectively, though I_{Na} showed graded reductions through the entire HCQ concentration range typified in a $22 \pm 1.8\%$ reduction at $1 \mu\text{M}$. No significant inhibition of I_{to} and I_{Ks} by μM -HCQ was observed.

Figure 2 presents the corresponding results obtained with AZM applied by itself similarly encompassing clinical therapeutic levels. However, the entire, 0-100 μM explored AZM concentration range yielded only minimal inhibitory effects. Even 10 μM and 100 μM AZM reduced I_{Na} (A), I_{CaL} , (B) I_{Ks} (E) and I_{Kr} (D) by $<17\%$ and $<35\%$ respectively and produced negligible effects on I_{K1} (F) and no effect on I_{to} (C). A previously reported dose regime administering 500, 250 and 250 mg/day on each of three successive days gave a day 2 serum concentration of $0.22 \mu\text{M}$ [35]. The effect of adding AZM on ionic channel currents accordingly adopted a higher concentration of 10 μM . Finally, Figure 3 summarizes results of applying the same range of five HCQ concentrations displayed in Fig. 1 now combined with 10 μM AZM. Adding AZM did not significantly alter the effects of HCQ on I_{Na} (A), I_{CaL} (B), I_{to} (C), and I_{Ks} (E), but reduced the IC_{50} for I_{Kr} ($\text{IC}_{50} = 7.7 \pm 0.8 \mu\text{M}$) and I_{K1} ($30.4 \pm 3.0 \mu\text{M}$).

Computational molecular docking studies exploring for HCQ-hERG and AZM-hERG interactions

The above findings, particularly concerning pharmacological effects on hERG, prompted computational molecular docking explorations for possible interactions between HCQ and AZM, and a recent hERG homotetramer structure (PDB ID: 5va2). Fig. 4 illustrates HCQ-hERG and AZM-hERG interactions suggested by the molecular docking studies. HCQ interacted predominantly with Y652 and F656 from one or more subunits (Fig.4B-D). Induced Fit Docking (IFD) protocol enabled HCQ to enter the space between the S5 and S6 helices. Other hERG residues involved in interactions with HCQ included F557, L622, T623, S624, and S660. Docking of AZM (Figure 4E-F) indicated similar, albeit less frequent interactions. This was reflected in an approximately two-fold weaker IFD score for AZM than for HCQ (-922 and -18340 for top-scoring positions, respectively). However, since docking scores can be biased toward larger ligands, it should be noted that comparing scores divided by the number of heavy atoms (i.e. non-hydrogen atoms) of each ligand would lead to over forty-fold differences in favour of HCQ rendering AZM a very weak binder. Variability in observed docking positions of ligands could be attributed to the highly symmetric structure of the hERG channel pore enabling many equivalent positions.

Electrical mapping and electrocardiographic studies in *ex vivo* cardiac preparations

We then explored the effects of HCQ alone and HCQ combined with AZM in intact Langendorff perfused whole hearts on electrophysiological activation and recovery, as well as consequent Ca^{2+} signalling processes reflecting excitation-contraction coupling. The recording and stimulation sites for these limited possible sites for further simultaneous electrocardiographic (ECG) monitoring. The latter adopted isolated heart single lead ECG recordings using one right atrial and one left ventricular recording electrode. These consequently did not correspond to the standard recording leads normally applied in intact animals as opposed to isolated hearts as opposed to intact animals. Nevertheless, the resulting traces permitted heart rates and PR and QRS durations to be followed, even if it was not possible to simply interpret apparent ST changes with HCQ and HCQ + AZM challenge, observed in 4 of 6 hearts studied.

Figure 5A summarises the sites of apical stimulation, and multi-electrode array (MEA) and ECG recording in the electrical mapping experiments. Representative left atrial (LA) and left ventricular (LV) isochronal conduction maps (B) obtained in the presence of 0 - 10 μM HCQ revealed a clear reduction of conduction velocity and increased conduction heterogeneities at 10 μM HCQ. Synergistic inhibitory effects on conduction velocity were observed when hearts were treated with the 10 μM HCQ in combination with 10 μM AZM. All these effects were reversed on drug washout (C(i)). 10 μM HCQ significantly decreased the conduction velocities of excitation with further decreases in velocity observed with the 10 μM HCQ and 10 μM AZM combination (C(ii)).

Quantification of the corresponding electrocardiogram (ECG) traces (D(i)) demonstrated that both 10 μM HCQ, and 10 μM HCQ in combination with 10 μM AZM, decreased heart rate (HR)(D(ii)), and increased PR interval (D(iii)) and QRS duration (D(iv)) related respectively to atrioventricular and ventricular conduction velocities. AZM combined with HCQ augmented the effects of HCQ on HR and PR interval. Together these results suggested that 10 μM HCQ, and 10 μM HCQ and 10 μM AZM combined, exerted synergistic inhibitory effects on heart rate and conduction.

Optical mapping studies in *ex vivo* cardiac preparations

We next investigated the effects of HCQ alone and in combination with AZM using optical fluorescence mapping in sinus-paced Langendorff-perfused hearts using the recording and ECG monitoring configurations illustrated in Fig. 6A(i). Voltage mapping measurements of action potential initiation and conduction (Fig. 6A(ii)) demonstrated bradycardic effects (A(iii)), visible conduction heterogeneities and slowed conduction (A(ii)) at 10 μ M HCQ, effects augmented by combination with 10 μ M AZM (Fig. 6A (iv)). Similarly, optical potentiometric mapping revealed that 10 μ M HCQ prolonged action potential duration at 90% repolarisation (APD₉₀) (B(i and ii)) with 10 μ M HCQ, effects further prolonged by its combination with AZM (Fig.5B(iii)). However, triggering phenomena, whether in the form of early or delayed afterdepolarization events, were not observed during the present experiments.

Ca²⁺ dye, Rhod-2 AM (CaD), mapping of ventricular calcium transient (CaT) characteristics demonstrated increased magnitudes of and dispersions in CaD durations at 90% recovery (CaD₉₀) (Fig. 6C(i)). The latter were attributed to changes late in the CaT records (C(ii)). The quantified CaD₉₀ magnitudes (B(iii)) and dispersions (B(iv)) both increased with 10 but not 1.0 μ M HCQ. The combination of 10 μ M HCQ with either 1 or 10 μ M AZM exerted significantly greater effects than 10 μ M HCQ alone. Final control experiments (D) compared (i) Ca²⁺ transients obtained in the presence of Rhod-2 alone, (ii) The positive and negative deflections representing the Ca²⁺ transients and the action potential timecourse during simultaneous Rhod-2 and Rh237 imaging, (iii) comparing their scaled timecourses. However, (iv) the Ca²⁺ transients showed similar and therefore uncontaminated timecourses whether they were studied with Rhod-2 alone or with Rhod-2 and Rh237 in combination.

Optical mapping assessments of arrhythmic tendency in *ex vivo* cardiac preparations

Finally, voltage dye optical mapping studies during ventricular pacing were used to assess susceptibility to arrhythmia induction before and after drug challenge in isolated perfused hearts (Fig.7A.B). Whilst 10 μ M HCQ did not exert detectable arrhythmic effects at the cycle lengths (CL) used, a combination of HCQ and AZM produced AP alternans at 180 ms CL and episodes of non-sustained torsadogenic-like VT at 170 ms CL in 5 out of 5 hearts. The corresponding potentiometric maps obtained during the colour-coded timepoints 1-6 are represented in (C). At a CL of 170 ms, the conduction maps with HCQ+AZM demonstrated significant disruptions of the normally coherent propagation of excitation waves with evidence of excitation re-entry and wave break. Thus, the electrophysiological changes outlined above

associated particularly with HCQ and AZM in combination were associated with a ventricular arrhythmic tendency.

Computational simulations of HCQ and AZM on human ventricular action potentials

To translate the experimental data describing the multi-ion channel blocking effects of HCQ and/or AZM to human ventricular excitation, the O'Hara-Rudy (Ord) model was implemented to reconstruct the impacts of HCQ alone and combined with AZM, on human ventricular action potentials including their APD₉₀ and maximal upstroke velocities on the basis of the individual channel patch-clamp data. Figure 8A displays predicted action potentials under control conditions and in the presence of HCQ, and HCQ and AZM combined. It was shown that with the 10 μ M HCQ alone, the APD was prolonged by 100 ms as compared to the control condition. With the combined action of HCQ and AZM, a synergistic action of the two drugs on APD prolongation was observed, manifested in a greater increase of APD₉₀ of ~300 ms (Fig. 8B). Such an APD prolongation can be attributed to the integrated action of reduced repolarisation potassium channel currents of I_{Kr} and I_{K1} , and reduced depolarising currents of I_{Na} , I_{CaL} and I_{NaCa} . A small reduction in action potential maximum upstroke velocities was also observed by both HCQ and HCQ+AZM due to the effects on I_{Na} , that could reflect small graded effects of HCQ on I_{Na} .

DISCUSSION

The present studies explored the electrophysiological effects of HCQ applied alone or with AZM, on individual voltage-gated ion channels under in vitro and in silico conditions, and on electrophysiological signalling in isolated Langendorff-perfused guinea-pig hearts. They thereby surveyed the successive levels of biophysical ion channel, molecular binding, electrophysiological AP conduction and recovery changes, and the related cytosolic $[Ca^{2+}]$ signalling for the first time. They then assessed for correlations between the experimental findings and O'Hara-Rudy (Ord) modelling predictions. Finally, they related the observed electrophysiological responses to drug challenge to the presence or absence of pro-arrhythmic changes. The latter were observed through disruptions in propagation of excitation, temporal action potential stability, and consequent torsade-like pro-arrhythmic changes in the intact hearts. This examination of the relationships between electrophysiological and potential

arrhythmogenic changes were prompted by clinical reports bearing on current interest in cardiac side effects of HCQ related to its use in Covid-19 therapy.

This resulting integrated clarification of HCQ and AZM action first explored their actions at the level of individual ion channel types. Here, these agents were tested on a range of specific human ion channel types expressed in patch-clamped HEK293 cells as recommended by CiPA guidelines [26]. We investigated cardiac ion channels responsible for the main inward (hNav1.5 (I_{Na}) Cav1.2 ($I_{Ca,L}$)) and outward (Kv4.3 (I_{to}), hERG (I_{Kr}), KCNQ1/E1 (I_{Ks}) and Kir2.1 (I_{K1})) currents in human ventricular myocardium. The HCQ and AZM both alone and in combination were applied systematically through wide concentration ranges encompassing and extending beyond reported therapeutic levels for the first time. At the upper limits of this concentration range, HCQ but not AZM significantly inhibited multiple human cardiac ion channels, particular hERG (mediating I_{Kr}) and Kir2.1 (I_{K1}), and, only to a lesser degree, hNav1.5 (I_{Na}). AZM potentiated the effects of HCQ on hERG and Kir2.1. Consistent with these experimental findings, computational molecular docking simulations utilizing a recent hERG homotetramer structure (PDB ID: 5va2) demonstrated a potential HCQ binding. This is predominantly with the Y652 and F656 from one or more hERG subunits. Additional residues involved in interactions with HCQ frequently included F557, L622, T623, S624, and S660. These findings merit closer mutagenesis studies confirming these suggested binding sites. In contrast, the model predicted substantially weaker AZM-hERG binding.

Secondly, some of the mapping studies examining effects of μ M-HCQ and (HCQ+AZM) at the level of intact perfused hearts yielded potentially important findings not anticipated from the above in vitro ion channel studies alone. They thus suggested alterations in action potential propagation patterns not directly predicted from the above biophysical results. Despite relatively minor effects of such concentrations on I_{Na} in the in vitro experiments, we demonstrated for the first time that μ M-HCQ reduced ventricular conduction velocities and increased their heterogeneities on multi-electrode array and RH237 optical voltage mapping. These findings accompanied compromised heart rates and slowed atrioventricular or intraventricular conduction, reflected in prolonged RR and PR intervals and QRS durations, emerging from ECG monitoring. Nevertheless these findings at the intact heart level parallel recent experimental reports that 1-3 μ M HCQ reduced heart rates, produced dose-dependent

reductions in hyperpolarization-activated currents (I_f), and further reduced I_{CaL} and I_{Kr} observed at 3 μ M HCQ [36]. Similar effects have been observed with clinical HCQ toxicity [37]. Clinical reports had also associated HCQ treatment with atrioventricular and bundle-branch block (incidence 0.01 to 0.1%) cf. [6]).

In contrast, the effects of HCQ in markedly increasing action potential durations and their heterogeneities, were compatible with the observed in vitro ion channel changes. O'Hara-Rudy modelling of human ventricular myocyte activity could correlate the observed action potential prolongations resulting from (HCQ+AZM) or HCQ challenge with their respective observed in vitro actions on I_{Kr} and I_{K1} . These observations also agreed with the established associations between HCQ challenge and prolonged action potential durations, clinically indirectly reflected in reported long QT intervals [3]. They also parallels a series describing case reports implicating both HCQ and AZM in prolonged QT interval and risk of torsade de pointes in long QT syndrome patients (<http://www.crediblemeds.org>; [38]).

Thirdly, we associated HCQ action with increased durations of cytosolic Ca^{2+} transients and their dispersions in intact perfused hearts during Rhod-2 optical mapping, effects similarly not demonstrable using in vitro ion channel studies. Fourthly, all these effects of HCQ, whether bearing on AP propagation, recovery, or Ca^{2+} signalling, were accentuated when HCQ was combined with AZM challenge. The latter findings associate the increased durations of the Ca^{2+} transients with the correspondingly increased APDs. This would be compatible with an accordingly prolonged AP plateau phase increasing Cav1.2 mediated Ca^{2+} influx that would in turn increase net Ca^{2+} induced SR Ca^{2+} release. Recent studies have suggested $[Ca^{2+}]_i$ feedback effects on Na^+ channel and gap junction function (Fig. 8C)[23, 25]. Thus, reductions in both I_{Na} and AP conduction velocity have accompanied both pharmacological conditions [27, 28] and genetic pro-arrhythmic models increasing abnormal RyR2-mediated Ca^{2+} release [29-31]. These feedback effects from Ca^{2+} homeostatic events were attributed to inhibitory actions of Ca^{2+} and calmodulin (CaM) binding on Nav1.5 channel binding sites [39, 40]. These might then account for the observed slowing of atrioventricular and ventricular action potential conduction with HCQ and (HCQ + AZM) challenge, findings not predicted by the in vitro patch clamp results.

The final experiments explored the extent to which the observed physiological effects produced arrhythmic effects as detected by voltage mapping in the intact Langendorff-perfused hearts studied here. Reduced AP conduction velocities and increases in conduction dispersion potentially generate re-entrant substrate. Prolonged APDs predispose to triggering early afterdepolarisations (EADs) during the ventricular AP plateau, classically attributed reactivation of I_{CaL} [41], itself increased by increased intracellular $[Ca^{2+}]$ and CaMKII mediated Cav1.2 phosphorylation [42]. The experiments applied forced pacing protocols whilst voltage mapping AP propagation patterns. However, they demonstrated that while combined (HCQ + AZM) challenge provoked alternans, ventricular tachycardic episodes, and re-entrant excitation, the electrophysiological changes following challenge with HCQ alone were not accompanied by pro-arrhythmic manifestations.

Translational correlates. The findings emerge with a novel mechanistic sequence in which action potential prolongation following HCQ-mediated K^+ channel downregulation alters Ca^{2+} homeostasis. This in turn may impact Na^+ channel function and AP conduction velocity [24, 25]. The final findings here parallel clinical reports describing electrophysiological changes in an absence of major cardiac arrhythmias (cf [12]) with therapeutic HCQ concentrations (cf. [11]), associated with rheumatoid arthritis, SLE and malarial prophylactic therapy. However, they signal a desirability of further studies exploring arrhythmic tendency particularly at higher HCQ dosages and especially if accompanied by AZM ([16]; cf.[17, 43]), or under other conditions associated with pre-existing arrhythmic substrate. The latter could include both *chronic* cardiac comorbidities as in diabetes, obesity, coronary artery disease, heart failure or cardiac arrhythmias or their medications, themselves associated with increased Covid-19 risk, or *acute* systemic malarial [22] or Covid-19 illness. The latter has been associated with prolonged action potentials and therefore QTc even without HCQ use (425-455 ms versus ~400 ms) as well as overt arrhythmic phenomena [21, 44], that could affect safety threshold HCG doses. This aligns the present physiological findings to the recent FDA guidelines bearing on cardiac safety in combined HCQ/AZM administration for Covid-19 treatment [4, 5, 16, 20], and the case for electrocardiographic, including QT, monitoring during 4-aminoquinoline-macrolide therapy for Covid-19 patients.

METHODS

Ethics and study Approval

All procedures were approved by The Institutional Animals Ethics Committees at Henan University, Kaifeng, China under and the national guidelines under which the institution operates, and also conform with the NIH Guide for the Care and Use of Laboratory Animals. Guinea pigs (male; 300-350 g) were provided by The Experimental Animal Center of the Medical College of Xi'an Jiaotong University and maintained in a pathogen-free facility at Henan University with *ad libitum* access to food and water. Animals were humanely sacrificed by intraperitoneal injection with 3% pentobarbital sodium (50 mg/kg).

Single-cell electrophysiological recordings

Core human cardiac channels were heterologously expressed in recombinant HEK293 or CHO cell lines and studied using conventional patch clamp methods. Stable cell lines expressing Nav1.5 and Cav1.2/ $\beta 2/\alpha 2/\delta 1$, hERG, Kir2.1, Kv4.3, KCNQ1/E1 were used. All currents were recorded using a MultiClamp 700A amplifier, 1550A digitizer and pCLAMP 10.6 software (Molecular devices, USA). Patch electrodes with resistances of 2-5 M Ω were pulled with a P-97 micropipette puller (Sutter Instruments, USA). The conventional whole-cell recordings were obtained by manual suction for hERG, Kir2.1, Kv4.3 and Nav1.5 studies. Perforated whole-cell recordings of KCNQ1/E1 and Cav1.2 were obtained following perforation with 200 μ g/ml amphotericin included in the pipette solution. After whole-cell mode were obtained, cells were used in voltage clamp mode for the current recordings. The external solution contained (mM): NaCl 137; MgCl₂ 1; KCl 4; glucose 10; HEPES 10; CaCl₂ 1.8, pH adjusted to 7.4 with NaOH. The K⁺-containing pipette solution contained (mM): KCl 40; KF 100; MgCl₂ 2; EGTA 5; HEPES 10, pH adjusted to 7.2 with KOH. The sodium and calcium current pipette solution contained (mM): CsCl 65; CsF 75; MgCl₂ 2.5; EGTA 5; HEPES 10, pH adjusted to 7.3 with CsOH.

Molecular modelling and docking studies

The experimental structure of the open hERG channel (PDB ID: 5va2) was selected as a receptor for molecular docking studies. The structure was prepared for docking with Protein Preparation Wizard on default settings including modelling of missing loops using Prime. The centroid of residues Y652 from every subunit was defined as the centre of the docking binding site. HCQ and AZM structures were obtained from PubChem and prepared for docking using LigPrep. Recently proposed Induced Fit Docking (IFD) protocol was used [45]. Protein

Preparation Wizard, LigPrep, Prime, and IFD were executed as parts of the Maestro software suite 2018-4 (Schrödinger, LLC, NY).

Langendorff- perfused isolated hearts

Guinea pigs (male; 300-350 g) were humanely killed by intraperitoneal injection with pentobarbital sodium (50 mg/kg). Hearts rapidly excised after thoracotomy were mounted onto a Langendorff perfusion system and perfused with a modified Tyrode's solution (119 NaCl, 25 NaHCO₃, 4 KCl, 1.2 KH₂PO₄, 1 MgCl₂, 1.8 CaCl₂·2H₂O, and 10 D-glucose (mM) equilibrated with 5% CO₂ and 95% O₂) with the flow rate of 8 ml/min at 37°C. Hearts were perfused and monitored for stability for 20 mins before experimental procedures commenced.

Electrical mapping of *ex vivo* cardiac preparations

A multi-electrode array (MEA) mapping system (EMS64-USB-1003, MappingLab Ltd., UK) was employed to record extracellular potentials (ECP) from the epicardium. Two 64-channel MEAs (MappingLab Ltd., UK) were employed for left atrial and left ventricular simultaneous recordings. ECP signals were recorded at a 10 kHz sampling using synchronized 64-channel EMS64-USB-1003 recording systems and recorded using EMapRecord 5.0 software (MappingLab Ltd., UK) and stored in a computer for subsequent off-line analysis. Electrocardiograms (ECG) were continuously recorded by two ECG electrodes (MappingLab Ltd., UK) positioned on the right atrium and left ventricle respectively. The epicardial isochronal activation map during sinus rhythm or imposed pacing was plotted as time differences between the earliest activation site and the individual activation site on each channel. Activation times were calculated as the point of maximal negative slope of activation waveforms. The conduction velocity (CV) was calculated from the difference in timing and the known distance between the recording points using EMapScope 5.0 software (MappingLab Ltd.).

Optical mapping of *ex vivo* cardiac preparations

After the Langendorff-perfused hearts reached steady state, contraction artefacts were minimized using blebbistatin (10 µM). Dye loading was aided by pre-perfusion with pluronic F127 (20 % w/v in DMSO). Rh237 (1 µg/ml) and Rhod2-AM (1 µg/ml) were perfused to enable simultaneous membrane potential and Ca²⁺ measurements at 37 °C. Two 530 nm LEDs

(LEDC-2001, MappingLab Ltd) were used to illuminate the heart after their emissions were bandpass filtered (wavelengths 530 ± 20 nm) to minimize stray excitation light reaching the dyes. The fluorescence light was passed through a 550 nm long-pass filter and then a dichroic mirror with a cut-off of 638 nm. Fluorescence light with wavelengths above 638 nm was passed through a 700 nm long-pass filter and then imaged by the camera for recording voltage signals. Fluorescence light below 638 nm was passed through a bandpass filter (585 ± 40 nm) then imaged by the camera for recording calcium signals (OMS-PCIE-2002, MappingLab Ltd). The raw spatial resolution was 128-by-128 pixels, the total mapping area was 16×16 mm and the temporal resolution was 900 frames/second. The cameras of the optical mapping system, LED lights and stimulator and ECG recording were simultaneously driven by an 8 channel TTL analog-digital converter and OMapRecord 4.0 software (MappingLab Ltd.). For the analysis of optical mapping signals and generation of isochronal maps, data were semi-automatically processed using OMapScope 5.0 software (MappingLab Ltd). In this experimental configuration, stable recordings for voltage (V_m) and intracellular Ca^{2+} (CaT) signals could be obtained for >2 hours in preliminary experiments assessing system stability.

Arrhythmia induction protocol

Stimuli were generated by an isolated constant voltage/current stimulator (VCS3001, MappingLab Ltd., UK). They were delivered with a platinum electrode onto the epicardial apex at an amplitude $1.5 \times$ the diastolic voltage threshold and a 2 ms pulse width. The optical mapping was performed in conjunction with an alternans mapping protocol. The heart was consecutively paced at basic cycle lengths (BCL) from 210 with 10 ms decrement until 170 ms. The heart was paced 50 times with 2 ms duration pulses and the optical mapping recording was performed at the last 2 second in each episode. This protocol was performed both before and after drugs were delivered.

In silico model reconstruction

The O'Hara-Rudy (ORd) human ventricular model [46] was modified to incorporate the actions on multi-channel block of HCQ, including the dose-dependent block of I_{Na} , I_{CaL} , I_{to} , I_{Kr} , I_{Ks} , I_{K1} and the Na^+-Ca^{2+} exchange current, I_{NCX} . This model was selected as it was developed from and validated against experimental data from human ventricular cells and found suitable for studying actions of drugs. The simulations evoked action potentials by a supra-threshold

stimulus in control runs and following application of HCQ, and combined application of HCQ and AZM. Action potential time courses characterized by AP durations at 90% repolarisation (APD₉₀) and maximal upstroke velocity (MUP) and the underlying ion channel currents targeted by the drugs were recorded for analysis.

Statistical analysis

All patch clamp recorded data were analyzed using Clampfit 10.6 (Molecular Devices, USA), OriginPro 8.0 (Origin Lab, USA) and Adobe Illustrator 10 (Adobe, USA). The concentration-response curve was fitted by the logistic equation $y = A_2 + (A_1 - A_2) / [1 + (x/x_0)^p]$, where x is the drug concentration, and p is the Hill coefficient. All data are expressed as the means \pm SEM. One-way ANOVA followed by multiple-comparison test was used to evaluate multiple test treatments. A value of $P < 0.05$ was considered statistically significant. IC₅₀ denotes the concentration determined for half-maximal inhibitory effects. In the figures, the designations for p values are: * $p < 0.05$, ** $P < 0.01$ and *** $P < 0.001$ respectively.

Sources of Funding

This work is supported by the Kaifeng Excellent Key Laboratory Grant (Grant no. 20190601A) British Heart Foundation (BHF) (PG/14/79/31102, and PG/15/12/31280 and BHF Centres for Research Excellence (CRE) at Cambridge, CLHH, PG/14/80/31106, PG/16/67/32340, ML, PG. FS/17/52/33113, AT) and Oxford (ML) the Chinese Natural Science Foundation (31171085: ML) and EPSRC (United Kingdom) (EP/J00958X/1 and EP/I029826/1) (HZ).

Disclosures

The authors have declared that no conflict of interest exists.

Author contributions

GH, CL, AT, DP, CLHH, HZ and ML contributed to the study design

GW, XT, GH, YN, LW, XJ, GH contributed to the electrophysiological data acquisition.

GW, YD, GH, YX, LW, DL and NH contributed to the data analysis and visualization.

HF, KZ, HZ contributed to the action potential computer simulation.

PM and ML contributed to the molecular docking computer simulation.

LW, DP, ML and GH contributed to the funding and resource acquisition.

ML and GH contributed to the supervision.

All authors contributed to the writing.

References

1. NIH, *NIH clinical trial of hydroxychloroquine, a potential therapy for COVID-19, begins*. 2020.
2. Pharmafield, *Novartis sponsors hydroxychloroquine clinical trial in hospitalised COVID-19 patients*, E. Morriss, Editor. 2020.
3. Hooks, M., et al., *Effects of hydroxychloroquine treatment on QT interval*. Heart Rhythm.
4. Chorin, E., et al., *The QT interval in patients with COVID-19 treated with hydroxychloroquine and azithromycin*. Nature Medicine, 2020.
5. Chorin, E., et al., *QT interval prolongation and torsade de pointes in patients with COVID-19 treated with hydroxychloroquine/azithromycin*. Heart Rhythm, 2020.
6. Costedoat-Chalumeau, N., et al., *Heart conduction disorders related to antimalarials toxicity: an analysis of electrocardiograms in 85 patients treated with hydroxychloroquine for connective tissue diseases*. Rheumatology (Oxford), 2007. **46**(5): p. 808-10.
7. White, N.J., *Cardiotoxicity of antimalarial drugs*. Lancet Infect Dis, 2007. **7**(8): p. 549-58.
8. Nosten, F., et al., *Cardiac effects of antimalarial treatment with halofantrine*. Lancet, 1993. **341**(8852): p. 1054-6.
9. Bouchaud, O., et al., *Fatal cardiotoxicity related to halofantrine: a review based on a worldwide safety data base*. Malar J, 2009. **8**: p. 289.
10. Godeau, P., et al., *[Disorders of conduction in lupus erythematosus : frequency and incidence in a group of 112 patients (author's transl)]*. Ann Med Interne (Paris), 1981. **132**(4): p. 234-40.
11. Chatre, C., et al., *Cardiac Complications Attributed to Chloroquine and Hydroxychloroquine: A Systematic Review of the Literature*. Drug Saf, 2018. **41**(10): p. 919-931.
12. Haeusler, I.L., et al., *The arrhythmogenic cardiotoxicity of the quinoline and structurally related antimalarial drugs: a systematic review*. BMC Medicine, 2018. **16**(1): p. 200.
13. Gautret, P., et al., *Hydroxychloroquine and azithromycin as a treatment of COVID-19: results of an open-label non-randomized clinical trial*. International Journal of Antimicrobial Agents, 2020: p. 105949.
14. Hinton, D., *Food and Drug Administration. FDA Emergency use authorization (EUA) of chloroquine and hydroxychloroquine*. . 2020, Food and Drug Administration. .
15. Lenzer, J., *Covid-19: US gives emergency approval to hydroxychloroquine despite lack of evidence*. BMJ, 2020. **369**: p. m1335.
16. Borba, M.G.S., et al., *Effect of High vs Low Doses of Chloroquine Diphosphate as Adjunctive Therapy for Patients Hospitalized With Severe Acute Respiratory Syndrome Coronavirus 2 (SARS-CoV-2) Infection: A Randomized Clinical Trial*. JAMA Network Open, 2020. **3**(4): p. e208857-e208857.
17. Lane, J.C.E., et al., *Safety of hydroxychloroquine, alone and in combination with azithromycin, in light of rapid wide-spread use for COVID-19: a multinational, network cohort and self-controlled case series study*. medRxiv, 2020: p. 2020.04.08.20054551.
18. Magagnoli, J., et al., *Outcomes of hydroxychloroquine usage in United States veterans hospitalized with Covid-19*. medRxiv, 2020: p. 2020.04.16.20065920.
19. Saleh, M., et al., *The Effect of Chloroquine, Hydroxychloroquine and Azithromycin on the Corrected QT Interval in Patients with SARS-CoV-2 Infection*. Circulation: Arrhythmia and Electrophysiology, 2020. **0**(13): p. e008662.
20. Mercuro, N.J., et al., *Risk of QT Interval Prolongation Associated With Use of Hydroxychloroquine With or Without Concomitant Azithromycin Among Hospitalized Patients Testing Positive for Coronavirus Disease 2019 (COVID-19)*. JAMA Cardiology, 2020.
21. Bhatla, A., et al., *COVID-19 and cardiac arrhythmias*. Heart rhythm, 2020. **17**(9): p. 1439-1444.

22. Chan, X.H.S., et al., *Factors affecting the electrocardiographic QT interval in malaria: A systematic review and meta-analysis of individual patient data*. PLoS Med, 2020. **17**(3): p. e1003040.
23. Huang, C.L., *Murine Electrophysiological Models of Cardiac Arrhythmogenesis*. Physiol Rev, 2017. **97**(1): p. 283-409.
24. Lei, M. and C.L.-H. Huang, *Cardiac arrhythmogenesis: a tale of two clocks?* Cardiovascular Research, 2019.
25. Lei, M., et al., *Modernized Classification of Cardiac Antiarrhythmic Drugs*. Circulation, 2018. **138**(17): p. 1879-1896.
26. Strauss, D.G., et al., *Comprehensive In Vitro Proarrhythmia Assay (CiPA) Update from a Cardiac Safety Research Consortium / Health and Environmental Sciences Institute / FDA Meeting*. Therapeutic Innovation & Regulatory Science, 2018. **53**(4): p. 519-525.
27. Li, M., et al., *Arrhythmic effects of Epac-mediated ryanodine receptor activation in Langendorff-perfused murine hearts are associated with reduced conduction velocity*. Clinical and experimental pharmacology & physiology, 2017. **44**(6): p. 686-692.
28. Valli, H., et al., *Epac-induced ryanodine receptor type 2 activation inhibits sodium currents in atrial and ventricular murine cardiomyocytes*. Clinical and Experimental Pharmacology and Physiology, 2018. **45**(3): p. 278-292.
29. Zhang, Y., et al., *Abnormal Ca(2+) homeostasis, atrial arrhythmogenesis, and sinus node dysfunction in murine hearts modeling RyR2 modification*. Front Physiol, 2013. **4**: p. 150.
30. Ning, F., et al., *The RyR2-P2328S mutation downregulates Nav1.5 producing arrhythmic substrate in murine ventricles*. Pflugers Arch, 2016. **468**(4): p. 655-65.
31. King, J.H., et al., *Loss of Nav1.5 expression and function in murine atria containing the RyR2-P2328S gain-of-function mutation*. Cardiovasc Res, 2013. **99**(4): p. 751-9.
32. Durcan, L., et al., *Hydroxychloroquine Blood Levels in Systemic Lupus Erythematosus: Clarifying Dosing Controversies and Improving Adherence*. J Rheumatol, 2015. **42**(11): p. 2092-7.
33. Miller, D.R., et al., *Plasma hydroxychloroquine concentrations and efficacy in rheumatoid arthritis*. Arthritis Rheum, 1987. **30**(5): p. 567-71.
34. Mégarbane, B., et al., *Blood concentrations are better predictors of chloroquine poisoning severity than plasma concentrations: a prospective study with modeling of the concentration/effect relationships*. Clin Toxicol (Phila), 2010. **48**(9): p. 904-15.
35. Lai, P.C., et al., *Azithromycin concentrations in blood and gingival crevicular fluid after systemic administration*. J Periodontol, 2011. **82**(11): p. 1582-6.
36. Capel, R.A., et al., *Hydroxychloroquine reduces heart rate by modulating the hyperpolarization-activated current I_f: Novel electrophysiological insights and therapeutic potential*. Heart rhythm, 2015. **12**(10): p. 2186-2194.
37. Marquardt, K. and T.E. Albertson, *Treatment of hydroxychloroquine overdose*. Am J Emerg Med, 2001. **19**(5): p. 420-4.
38. Roden, D.M., et al., *Considerations for Drug Interactions on QTc in Exploratory COVID-19 (Coronavirus Disease 2019) Treatment*. Circulation, 2020. **141**: p. e906-e907.
39. Sarbjit-Singh, S.S., H.R. Matthews, and C.L.H. Huang, *Ryanodine receptor modulation by caffeine challenge modifies Na⁺ current properties in intact murine skeletal muscle fibres*. Scientific Reports, 2020. **10**(1): p. 2199.
40. Young, K.A. and J.H. Caldwell, *Modulation of skeletal and cardiac voltage-gated sodium channels by calmodulin*. J Physiol, 2005. **565**(Pt 2): p. 349-70.
41. January, C.T. and J.M. Riddle, *Early afterdepolarizations: mechanism of induction and block. A role for L-type Ca²⁺ current*. Circ Res, 1989. **64**(5): p. 977-90.
42. Herring, N., M. Kalla, and D.J. Paterson, *The autonomic nervous system and cardiac arrhythmias: current concepts and emerging therapies*. Nat Rev Cardiol, 2019. **16**(12): p. 707-726.
43. Darpö, B., *Spectrum of drugs prolonging QT interval and the incidence of torsades de pointes*. European Heart Journal Supplements, 2001. **3**(suppl_K): p. K70-K80.
44. Wang, D., et al., *Clinical Characteristics of 138 Hospitalized Patients With 2019 Novel Coronavirus-Infected Pneumonia in Wuhan, China*. JAMA, 2020. **323**(11): p. 1061-1069.

45. Sherman, W., H.S. Beard, and R. Farid, *Use of an Induced Fit Receptor Structure in Virtual Screening*. Chemical Biology & Drug Design, 2006. **67**(1): p. 83-84.
46. O'Hara, T., et al., *Simulation of the undiseased human cardiac ventricular action potential: model formulation and experimental validation*. PLoS Comput Biol, 2011. **7**(5): p. e1002061.

Figure legends

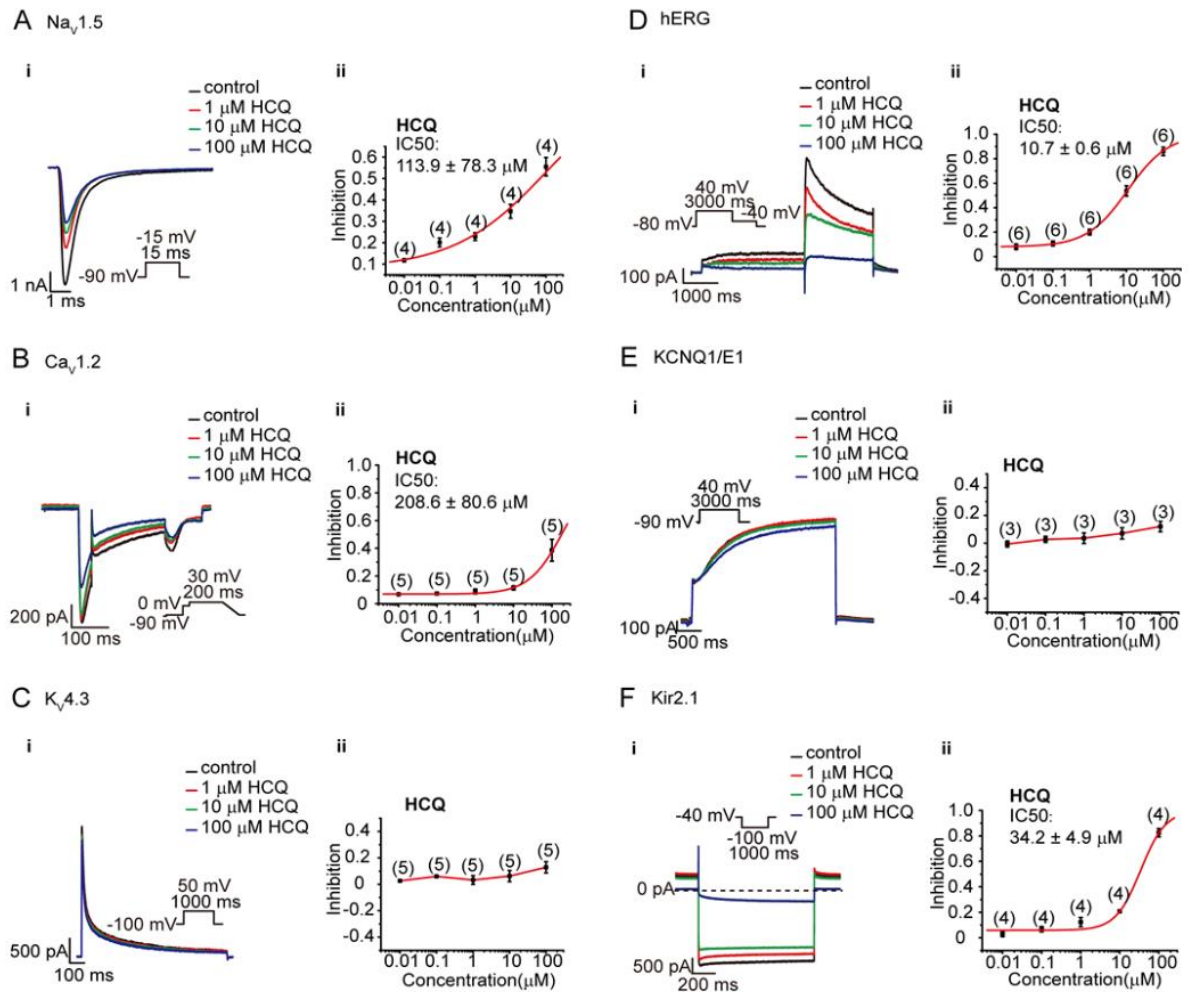


Figure 1. Effects of HCQ on ion currents attributable to hNav1.5 (I_{Na} , A), Cav1.2 ($I_{\text{Ca,L}}$, B), Kv4.3 (I_{to} , C), hERG (I_{Kr} , D), KCNQ1/E1 (I_{Ks} , E) and Kir2.1 (I_{K1} , F). (A-F) Left panels (i): Typical currents in the presence of 0, 1, 10 and 100 μM HCQ. Insets summarize the voltage clamping protocols. Right panels (ii): Mean concentration-response plots constructed for the maximum magnitude of each current (n cells).

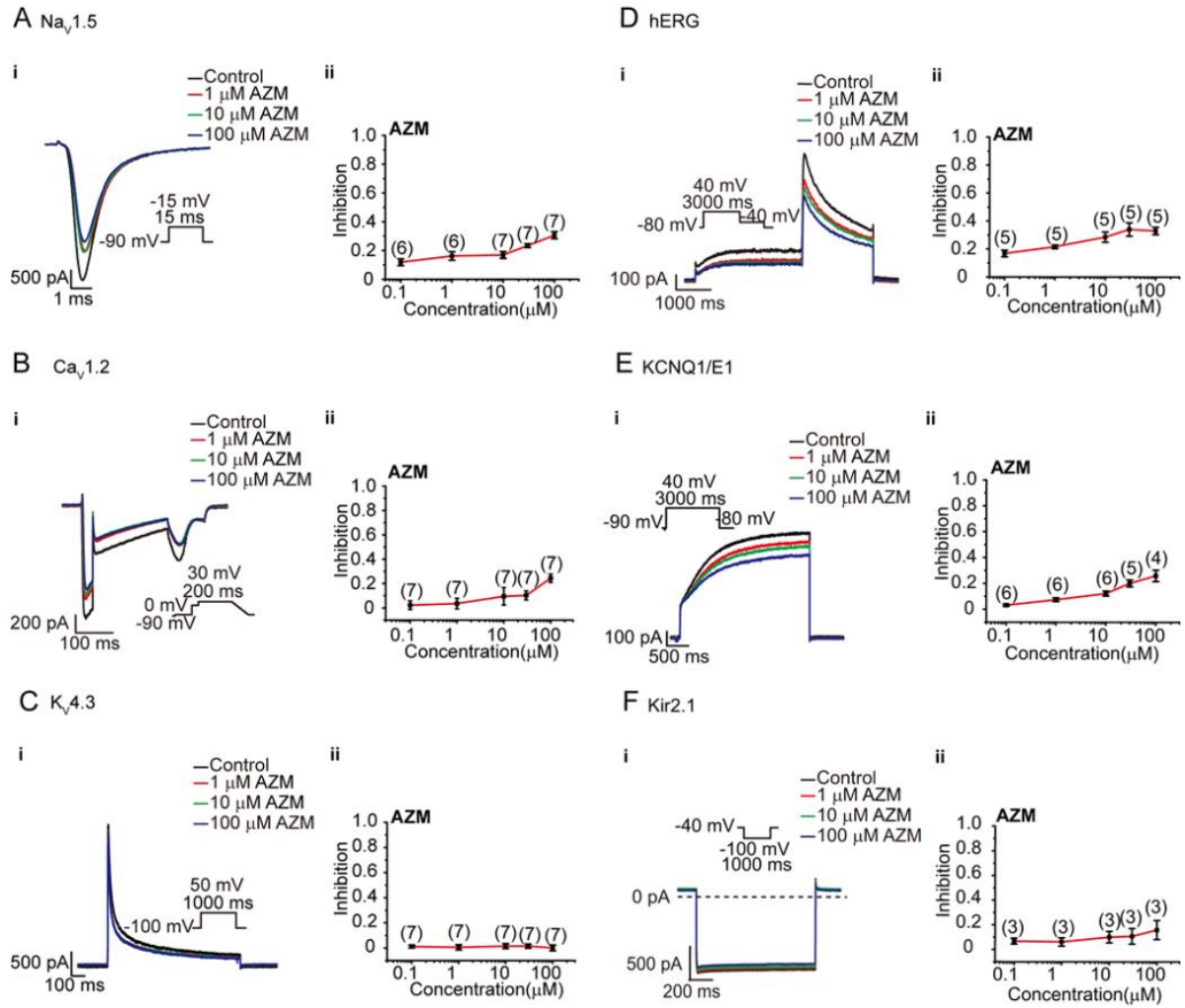


Figure 2. Effects of AZM on ion currents attributable to hNav1.5 (I_{Na} , A), Cav1.2 ($I_{Ca,L}$, B), Kv4.3 (I_{to} , C), hERG (I_{Kr} , D), KCNQ1/E1 (I_{Ks} , E) and Kir2.1 (I_{K1} , F). (A-F) Left panels (i): Typical currents in the presence of 0, 1, 10 and 100 μM HCN. Insets summarize the voltage clamping protocols. Right panels (ii): Mean concentration-response plots constructed for the maximum magnitude of each current ((n cells).

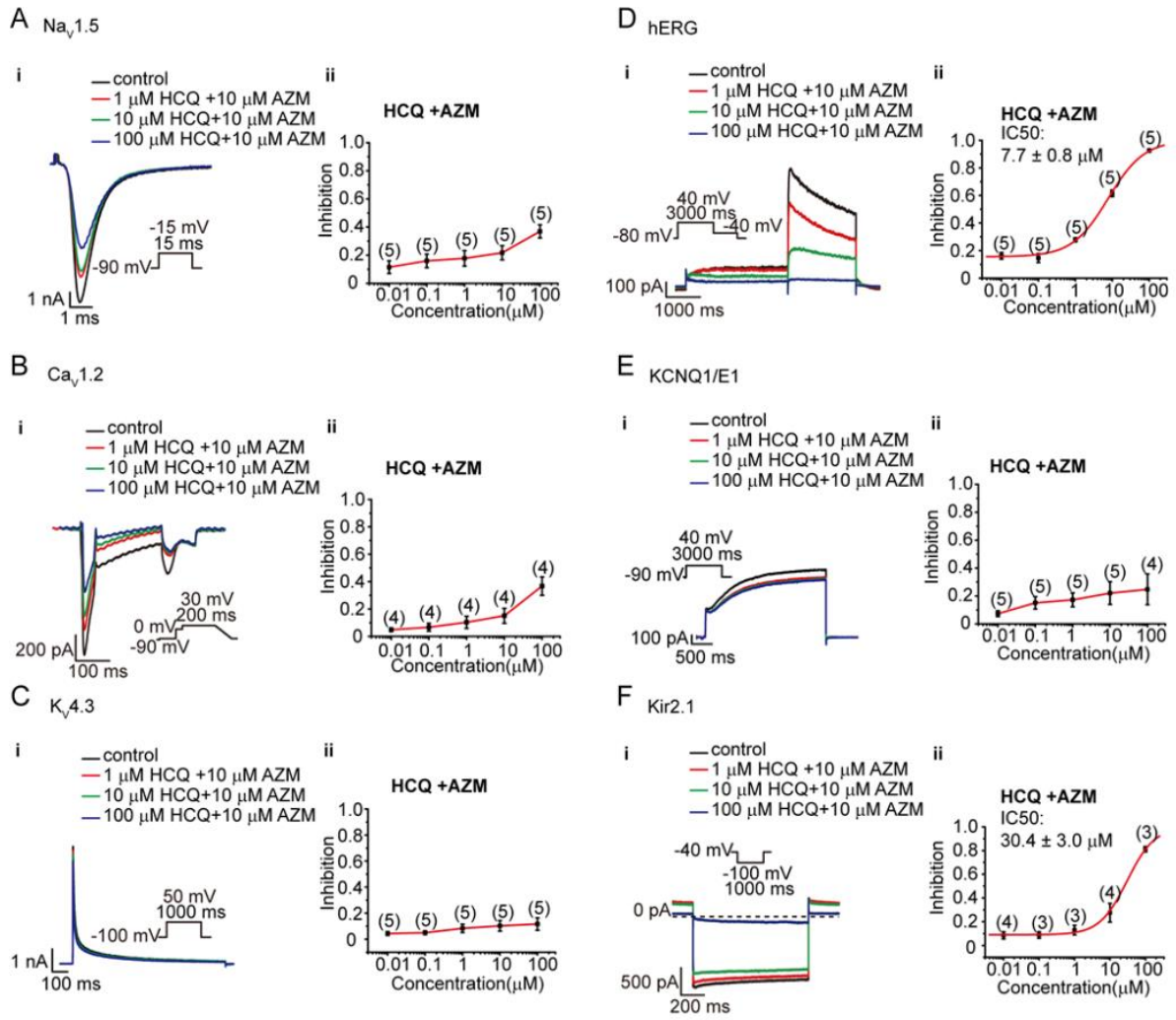


Figure 3. Effects of HCQ in combination with 10 μM AZM on ionic currents attributable to hNav1.5 (I_{Na} , A), Cav1.2 ($I_{Ca,L}$, B), Kv4.3 (I_{to} , C), hERG (I_{Kr} , D), KCNQ1/E1 (I_{Ks} , E) and Kir2.1 (I_{K1} , F). (A-F) Left panels (i): Typical currents in the presence of 0, 1, 10 and 100 μM HCQ with 10 μM AZM. Insets summarize the voltage clamping protocols. Right panels (ii): Mean concentration-response plots constructed for the maximum magnitude of each current (n cells).

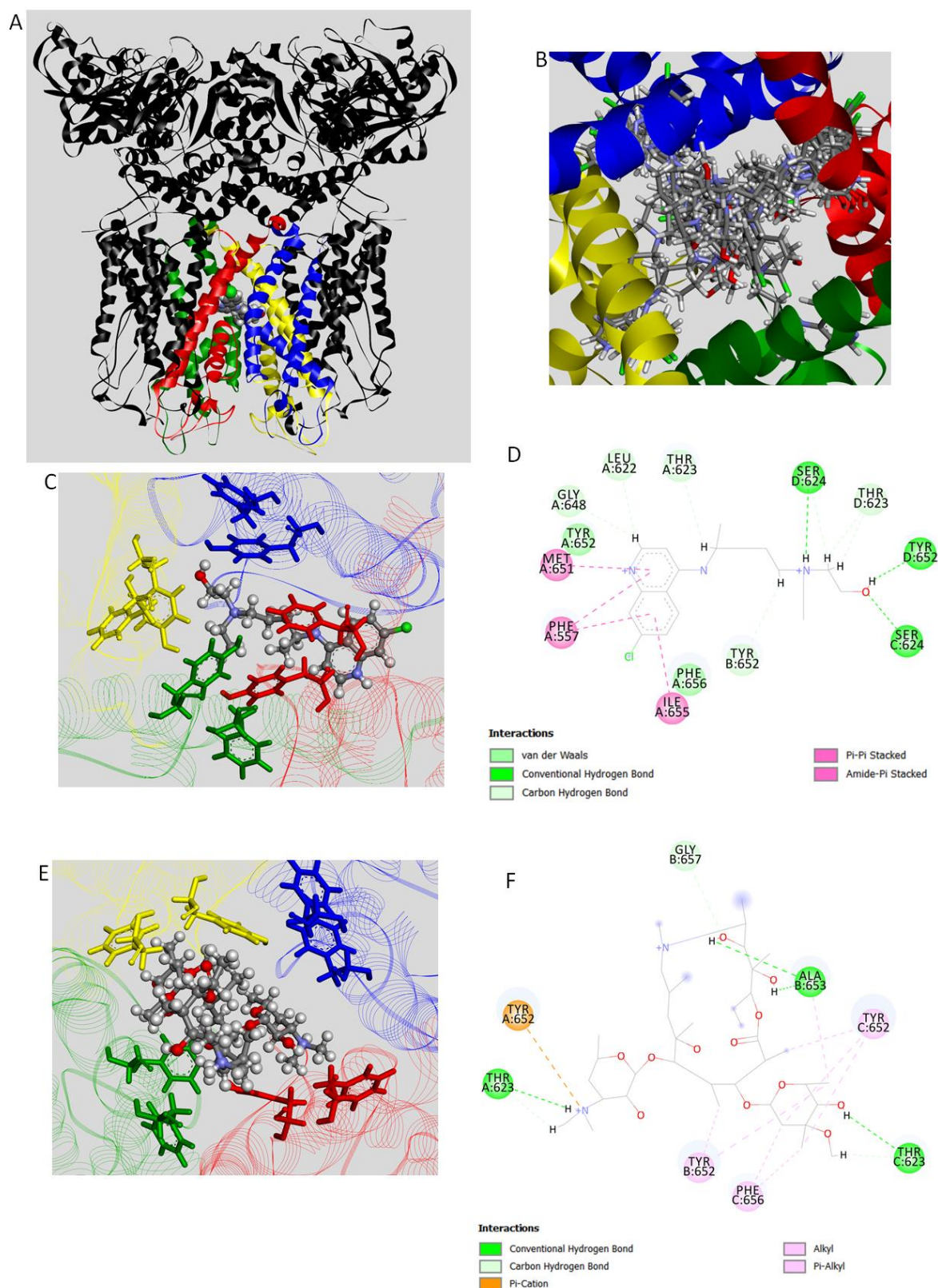


Figure 4. Computational docking studies. (A) hERG homotetramer structure (PDB ID: 5va2) with HCQ molecule (space-filling representation) indicating binding site placement. Residues 544-671 used in IFD of hERG chains A, B, C, and D colored red, green, yellow, and blue, respectively. (B) Overlay of IFD HCQ positions. (C) Representative, top-scoring positions of HCQ (ball-and-stick). Y652 and F656 residues in stick representation colored accordingly to

their parent chains. (D) 2-dimensional (2D) diagram depicting interaction types between presented HCQ position and hERG. (E) Representative, top-scoring position of AZM, and (F) 2D diagram depicting AZM-hERG interactions. Diagrams were prepared using Non-bond Interactions Monitor tool in Discovery Studio Visualizer (Dassault Systèmes, Vélizy-Villacoublay, France). IFD = Induced Fit Docking.

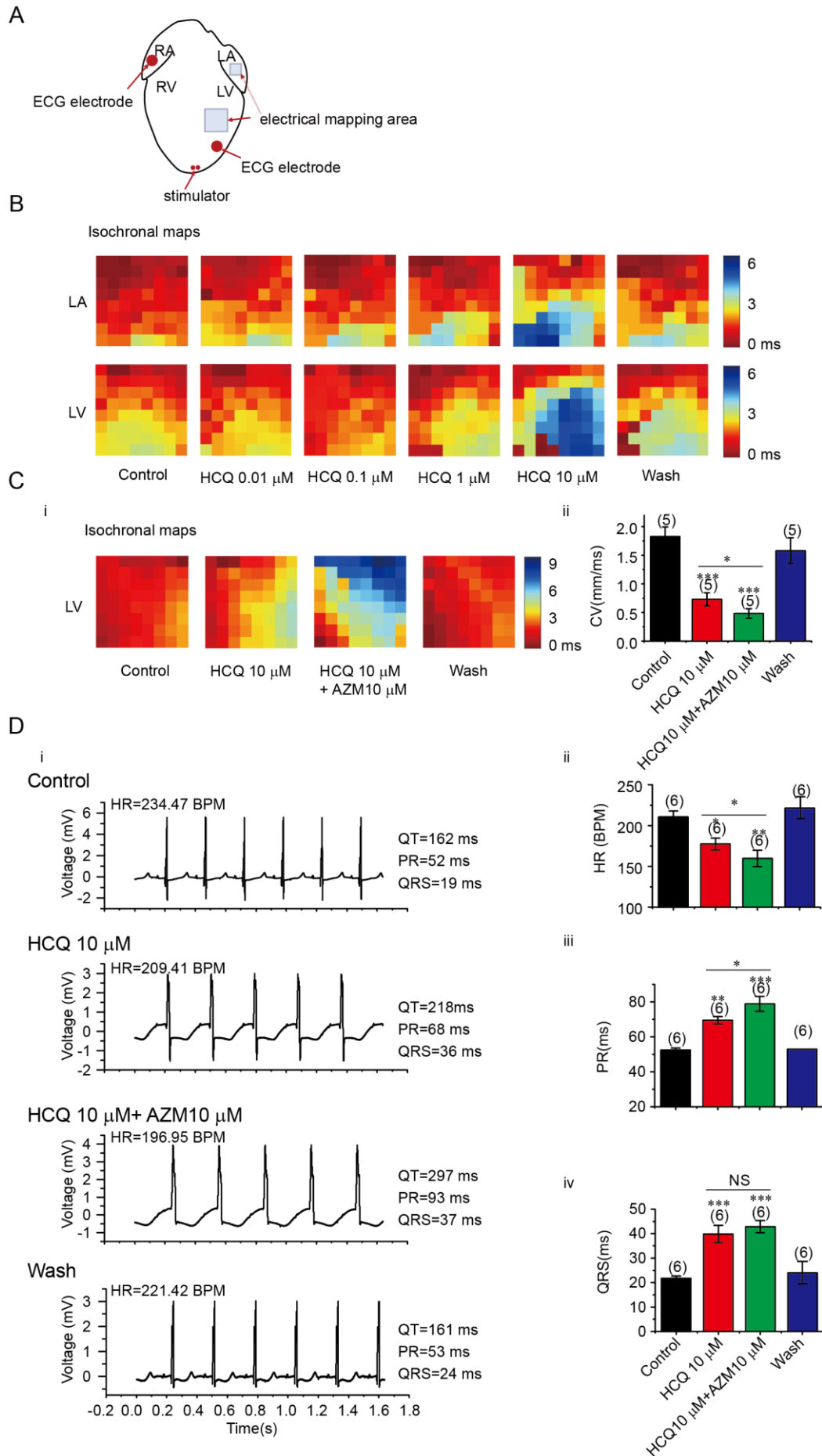


Figure 5. Multi-electrode array (MEA) mapping and electrocardiographic (ECG) studies in isolated perfused guinea-pig hearts following HCQ and AZM challenge. (A) Schematic summary of stimulation and MEA and ECG recording configuration. (B) Typical left atrial and left ventricular isochronal conduction maps obtained in the presence of 0, 0.01, 0.1, 1.0 and 10 μ M HCQ. (C) (i) Successive LV isochronal maps before and following addition of 10 μ M HCQ and 10 μ M HCQ and 10 μ M AZM in combination followed by drug washout. (ii) Quantified conduction velocities through these conditions. (D) ECG studies: (i) ECG records obtained before and following application of 10 μ M HCQ, and 10 μ M HCQ and 10 μ M AZM combined, followed by drug washout. (ii)-(iv): corresponding measured (ii) heart rates (HR), (iii) PR intervals and (iv) QRS durations (n hearts) * $P < 0.05$, ** $P < 0.01$, *** $P < 0.001$.

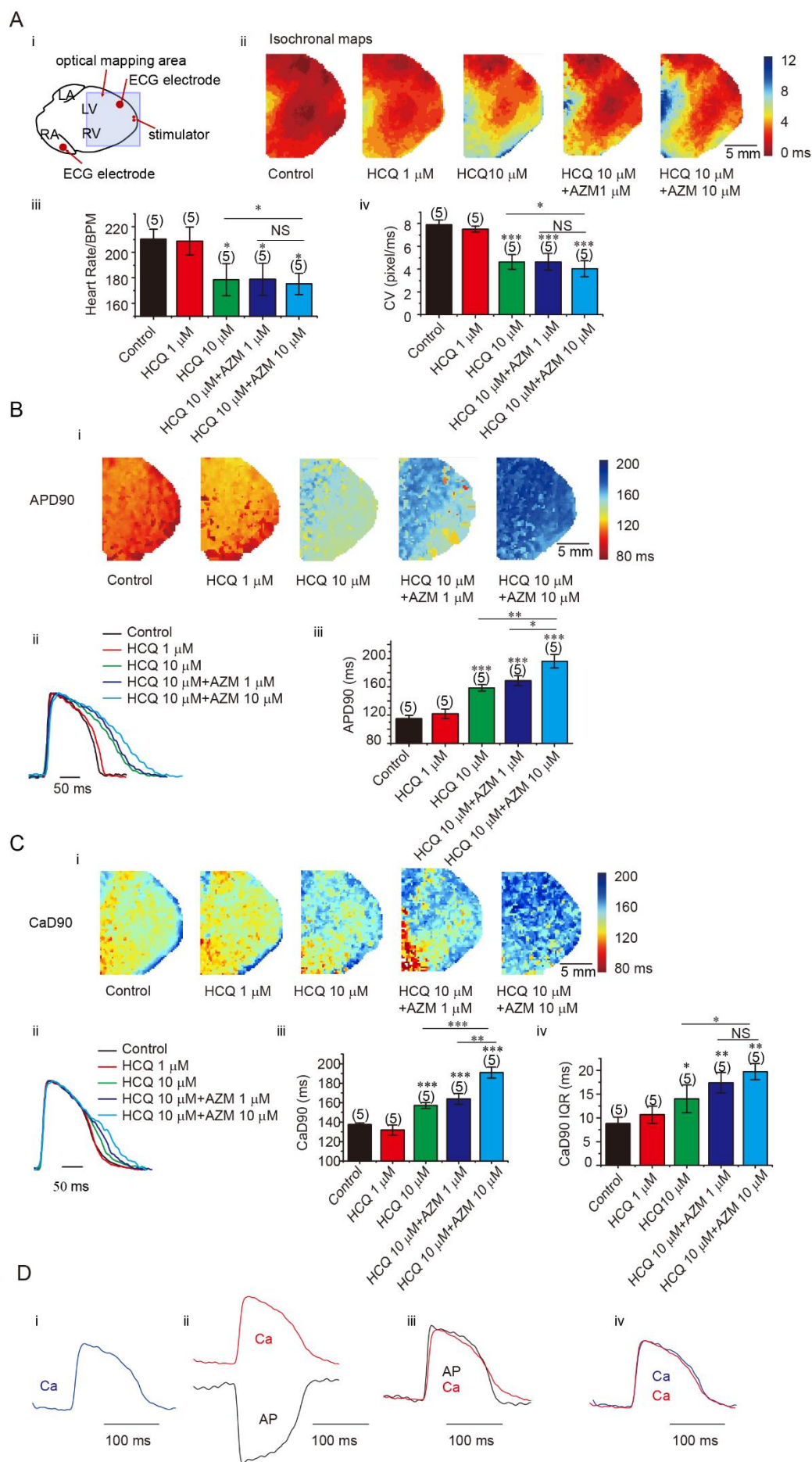


Figure 6. Voltage RH237 and Rhod-2 optical mapping in isolated perfused hearts. Comparisons of results before and following challenge by 1 μ M and 10 μ M HCQ, and 10 μ M HCQ combined with either 1 or 10 μ M AZM. (A, B) RH237 mapping: (A)(i) Optical mapping and ECG monitoring configuration (ii) Maps of action potential initiation and conduction; (iii) heart rates and (iv) conduction velocities. (B) Action potential time-courses and recoveries: (i) Maps of AP durations at 90% repolarization (APD₉₀). (ii) Representative APs recorded from defined regions of interest. (iii) APD₉₀s averaged over the field of view. “ (C) Rhod-2 AM (CaD) mapping of ventricular Ca²⁺ transients (CaT): (i) maps of CaD durations at 90% recovery (CaD₉₀). (ii) Comparison of typical CaT transients averaged over defined regions of interest; (iii) CaD₉₀ magnitudes; (iv) CaD₉₀ dispersions (n hearts). (D) (i) Ca²⁺ transients obtained in the presence of Rhod-2 alone, (ii) Ca²⁺ transients and the action potential timecourse during simultaneous Rhod-2 and Rh237 imaging, and (iii) a comparison of their scaled timecourses (iv) Comparison of Ca²⁺ transients studied with Rhod-2 alone or with Rhod-2 and Rh237 in combination. NS not significant, * P<0.05, ** P<0.01, *** P<0.001.

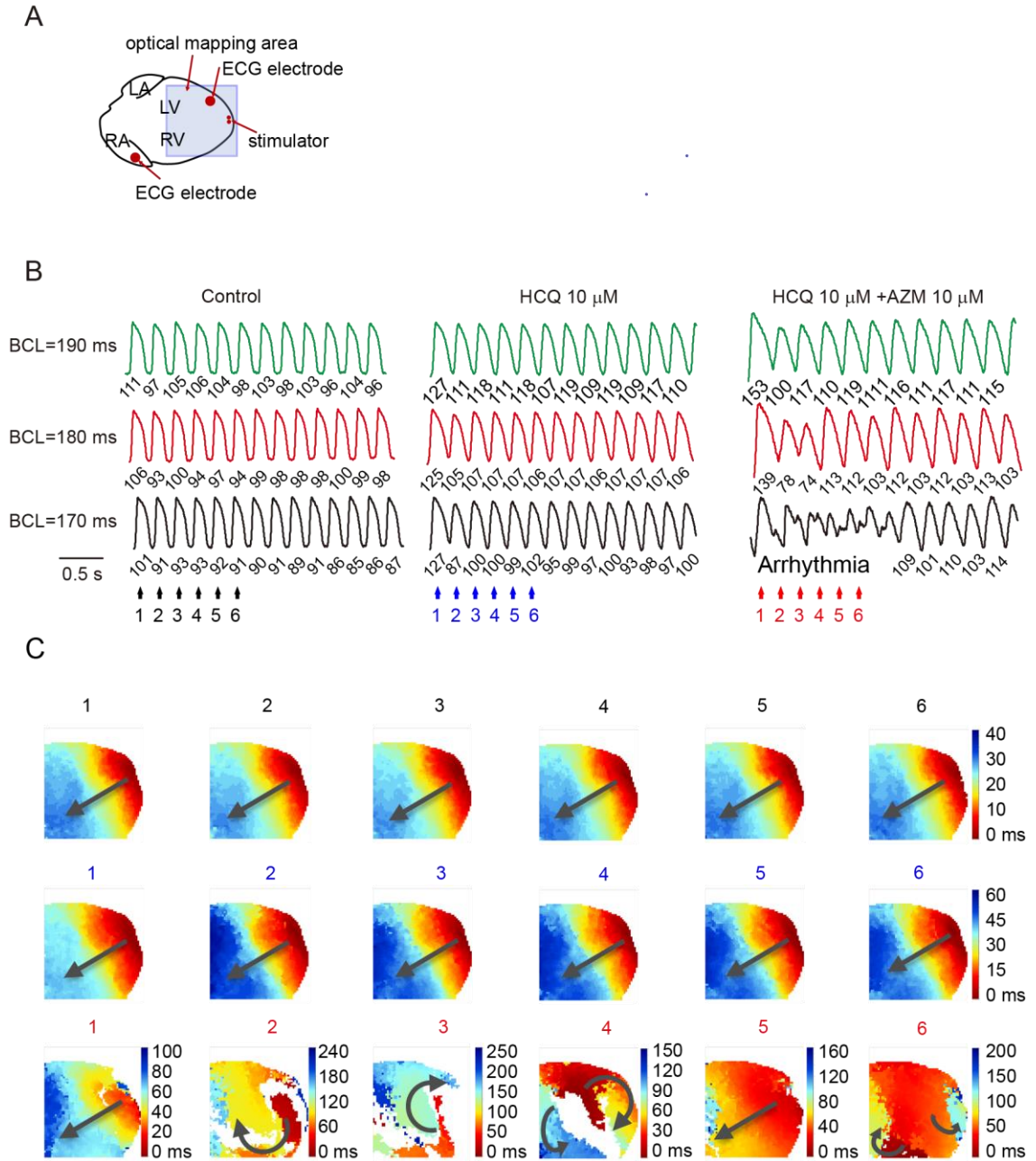


Figure 7. Voltage RH237 optical mapping of re-entry and ventricular arrhythmic tendency in isolated perfused hearts. (A) Recording and programmed stimulation configuration. (B) Optical action potential traces obtained under programmed pacing at 190 ms, 180 ms and 170 ms cycle lengths (CLs), before (control) and following addition of 10 μ M HCM, and 10 μ M HCM with added 10 μ M AZM. (C) Corresponding voltage maps obtained at the numbered colour-coded timepoints (n hearts).

and possible mechanisms underlying the pro-arrhythmic effects of applications of HCQ and HCQ and AZM combined at the ion channel, cellular and tissue levels.

